THE ASTROPHYSICAL JOURNAL, 416:185–203, 1993 October 10

THE STELLAR POPULATION IN THE ρ OPHIUCHI CLUSTER[1]

F. COMERON,[2] G. H. RIEKE,[3] A. BURROWS,[4] AND M. J. RIEKE[5]

Received 1992 July 31; accepted 1993 March 29

ABSTRACT

We report a near-infrared survey of 200 arcmin^2 in the cores of the ρ Ophiuchi interstellar clouds, leading to the detection of 91 sources. We develop a new method for estimating the luminosities of these sources based on fitting of isochrones from theoretical models. Application of this method allows us to determine a luminosity function and accompanying initial mass function for the cluster of young stars forming in these clouds. The IMF extends to well below the bottom of the main sequence (0.08 $M_\odot$) with no obvious feature at the transition between stellar and substellar masses. The power-law exponent of the IMF at low stellar and substellar masses is roughly -1.3 to -1.1, with formal errors of 0.2. These values are consistent with extrapolation of many estimates of the local IMF to substellar masses. At least seven objects appear to be substellar, even allowing for the largest plausible errors in the observations, the analysis, and the theoretical evolutionary models for these sources. It therefore seems likely that brown dwarfs form in significant numbers and that the process of cloud fragmentation is not biased against substellar masses. These results indicate that the widespread difficulty in finding large numbers of brown dwarfs in older stellar populations arise from the rapid cooling and possibly from atmospheric absorptions that may depress the near infrared spectra outputs of these objects.

Subject headings: open clusters and associations: individual (ρ Ophiuchi) — stars: low-mass, brown dwarfs — stars: luminosity function,mass function

1. INTRODUCTION

Studies of the form of the initial mass function, particularly ones that extend down to low-mass stars and substellar objects, are important to set observational constraints on issues such as the mechanisms for fragmentation of interstellar clouds and the accretion processes leading to star formation (Shu, Adams, & Lizano 1987; Liebert & Probst 1987). However, searches for very low mass objects are frustrated by their intrinsically low luminosity and by the low surface temperatures which make them radiate mostly at near-infrared wavelengths. A variety of techniques have been applied, including use of proper motions (Luyten 1968), objective prism spectra (Reid 1982), or photometric colors (Reid & Gilmore 1982). Candidate low-mass companions of nearby stars have been discovered by astrometric or radial velocity measurements, by speckle infrared interferometry, and by infrared photometry (see review by Stevenson 1991). The result of these efforts is the demonstration that, even within 10 pc of the Sun, searches for the lowest mass stars may remain incomplete, while few if any substellar objects have been found (Stevenson 1991).

A different approach is based on the existence of special conditions that would render these low-mass objects easier to detect. Low-mass objects in regions of recent star formation will be in early phases of contraction and will have radii and surface temperatures and hence luminosities far in excess of those characteristic of similar objects later in their evolution. Consequently, searches for low-mass objects have been conducted in nearby open clusters such as the Hyades (Leggett & Hawkins 1989; Hubbard, Burrows, & Lunine 1990) and the Pleiades (Stauffer et al. 1989; Hambly, Hawkins, & Jameson 1991). The availability of very sensitive ground- and space-based infrared detectors in recent years has made it possible to study regions containing even younger stellar populations, such as the Taurus dark clouds (Elias 1978b; Kenyon et al. 1990; Beichman, Boulanger, & Moshir 1992), Monoceros R2 (Beckwith et al. 1976), the Orion molecular clouds (Genzel & Stutzki 1989), the Chamaeleon dark clouds (Gauvin & Strom 1992), the Serpens molecular cloud (Eiroa & Casali 1992), and the NGC 2023/2024/2068/2071 complex (Lada et al. 1991). The properties of embedded clusters have been reviewed by Lada & Lada (1991).

The ρ Ophiuchi molecular cloud is an unusually propitious site for studying the formation of low mass stars. It is one of the molecular clouds closest to the Sun. It is located at the very young northern end of the Upper Scorpius group of the Scorpius OB2 association (Blaauw 1964; de Geus 1992) and is the most prominent concentration in a zone containing other minor star-forming regions (Herbst & Warner 1981). This complex marks the edge of the Gould's Belt ensemble of recent star formation tracers (Stothers & Frogel 1974) above the Galactic plane. The compact core of this cloud contains a high density of gas and dust with a visual extinction in excess of $A_V = 50$ mag and a mass of 550 $M_\odot$ (Wilking & Lada 1983). The many infrared surveys of the embedded stellar population (e.g., Grasdalen, Strom, & Strom 1973; Vrba et al. 1975; Fazio et al. 1976; Vrba, Strom, & Strom 1976; Elias 1978a; Chini 1981; Wilking & Lada 1983; Young, Lada, & Wilking, 1986; Myers et al. 1987; Wilking, Lada, & Young 1989, hereafter WLY; Rieke, & Ashok 1989; Barsony et al. 1989; Rieke & Rieke 1990; and Greene & Young 1992) reveal the existence of a probably bound stellar cluster with an age $\leq 3 \times 10^6$ yr.

[1] Observations reported in this paper were obtained with the Multiple Mirror Telescope, operated by the Smithsonian Astrophysical Observatory and the University of Arizona.

[2] Department of Astronomy and Meterology, University of Barcelona, E-08028 Barcelona, Spain; visiting Steward Observatory, University of Arizona.

[3] Steward Observatory and Department of Planetary Sciences, University of Arizona, Tucson, AZ 85721.

[4] Department of Physics, University of Arizona, Tucson, AZ 85721.

[5] Steward Observatory, University of Arizona, Tucson, AZ 85721.

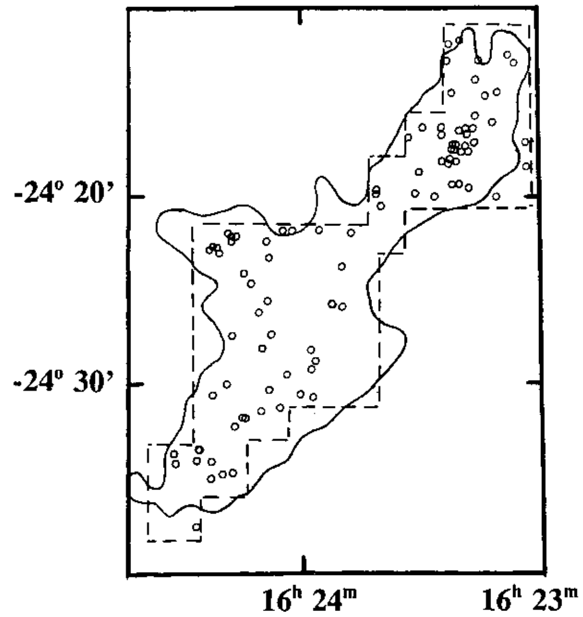

FIG. 1.—Map of the ρ Ophiuchi cloud indicating the $A_V = 50$ contour (from Wilking & Lada 1983). The area within the dashed box is covered in the present study. Positions of sources detected in the survey are plotted in this box.

These studies give a reasonably complete picture of the moderate and high mass members of this cluster. The cloud is nearby (160 pc), so available instrumentation has adequate angular resolution and sensitivity to identify individual low mass objects and study them in some detail.

Although their detectability should be increased, unambiguous recognition of low-mass stellar objects in star forming regions such as ρ Ophiuchi is complicated by several factors, such as the extinction in the cloud, the existence of substantial amounts of circumstellar material, and the diversity of evolutionary states (Adams & Shu 1986; Adams, Lada, & Shu 1987). Moreover, theoretical uncertainties exist in modeling both the interiors and the atmospheres of low-mass objects (Liebert & Probst 1987; Stevenson 1991). Nevertheless, extensive work in recent years has improved the equations of state, opacities, and numerical techniques used in these models (e.g., D'Antona & Mazzitelli 1985; Lunine, Hubbard, & Marley 1986; Burrows, Hubbard, & Lunine 1989; Burows et al. 1993). Combined with adequate observational material, the increasingly reliable models should allow us to draw potentially important conclusions regarding the existence and abundance of low-mass objects. At the same time, the analysis of observational data may provide insights into the reliability of the theoretical models.

In this paper, we present a high-sensitivity infrared survey of the core of the ρ Ophiuchi cloud. A preliminary discussion of a number of very low luminosity objects in this survey has been published elsewhere (Rieke & Rieke 1990). This paper describes the entire stellar population, integrating the low-mass members with the rest of the population in a consistent fashion. The survey is analyzed in terms of the initial mass function for this region and its implications for the evolutionary status of the forming cluster. We discuss the reliability of the evolutionary models for the young, embedded objects and analyze any effects modeling uncertainties would have on our conclusions. We show that the new data permit construction of an IMF that extends from masses well below the bottom of the main sequence up to $\simeq 7\,M_\odot$.

2. NEW OBSERVATIONS

We have used the Steward Observatory 2.3 m telescope to obtain a deep survey of the ρ Ophiuchi molecular cloud at H (1.6 μm) and K (2.2 μm). The observations used a NICMOS2 128 × 128 array of HgCdTe detectors, manufactured by Rockwell International Science Center. This array is mounted in a camera that provides for cold baffling at a pupil and projects each pixel to a scale of 1".27 on the sky (as measured during these observations), providing a total field of view of 2'.7. Guiding is through a dichroic mirror that allows a visible image for the acquisition TV of the identical field being observed in the infrared.

Measurements were obtained by offsetting the telescope to the nominal position and exposing for roughly 60 s. The telescope was next wobbled to a position 2'.4 to the south, where another 60 s exposure was obtained. The telescope was then returned to the first position and the process repeated until an adequate ratio of signal-to-noise had been achieved. Frame pairs were spaced by 2'.4 in right ascension. The measurements reported in this paper were obtained 1989 May 22–25 (U.T.). Combined with the survey reported by Rieke, Ashok, & Boyle (1989), we have completed deep surveys of a total of about 200 arcmin^2 in the ρ Ophiuchi molecular cloud. These observations have been concentrated on the cores of the cloud; the region surveyed is indicated in comparison with the $A_V > 50$ mag contour from Wilking & Lada (1983) in Figure 1.

Following the camera observations, we obtained aperture photometry of all sources brighter than $m_K = 14.5$ within the $A_V = 50$ contour and which had not been measured by previous authors (excepting a small number of cases where source confusion made it impossible for us to make reliable measurements). This photometry used the Multiple Mirror Telescope and the facility infrared photometer, which employs a helium-cooled InSb detector. We used an aperture of 5".4 and a chopper throw of 10" in elevation. Measurements were made at J (1.25 μm), H, K, and L' (3.4 μm), except where low signal-to-noise ratios made measurements prohibitively slow. Virtually all of these measurements were obtained 1991 April 26–28; a few confirming observations were made on 1992 April 14. Each source was measured in all colors in a period of 30 minutes or less.

A limited area of the ρ Ophiuchi area was imaged to greater depth than our overall survey by using a NICMOS3 256 × 256 array on the 2.3 m telescope on 1991 May 5–6. This array is used in the identical camera employed for the earlier measurements with the NICMOS2. The pixel scale was set to 0".6, so that the field of view was 2.6 arcmin square. Small telescope motions were made between exposures so that a flat field could be constructed by median averaging the set of exposures in a given field, with a net field of about 2.3 arcmin square that had full coverage. Three fields were observed, resulting in a deep sampling of 15 arcmin^2.

3. DATA REDUCTION

The instrumental signature was removed from the imaging data by (1) subtracting an electronic offset frame obtained by blocking all external signals to the array; (2) removing bad pixels by replacing them with the average signal for the surrounding detectors (the NICMOS2 array has less than 0.5% bad pixels); (3) ratioing the frames obtained at complementary telescope positions to obtain a flat-fielded result; and (4) multiplying the result by the mean sky level determined from the frames. There were generally no suitable guide stars at the positions observed; hence, before combining frames obtained at the same position, we centroided detected sources and used their positions to shift the frames to coincide exactly. The result of these processing steps is a flat-fielded frame set in which sources lying in northern fields of view appear as positive above the sky level and sources lying in the southern fields fall below this level. Occasionally two sources will be superimposed and the fainter will not be detected; from the resolution (1''.27) and source density (one source per 7000 arcsec^2 on average), this problem should occur rarely. These processing steps were performed with dedicated software on an 80386-based computer.

After these initial processing steps, the frames were transfered to a SUN computer and subsequent reductions were under IRAF. Within IRAF, we used the DAOFIND routine to identify the sources on the frames. We experimented with various settings of the input parameters until a set was determined that provided reliable and repeatable extractions. The reliability was judged both by visible identification of likely sources and the robustness of the procedure when small changes were made in the input parameters. The extracted sources were measured with APPHOT. Again, the input parameters were adjusted carefully to provide high internal consistency in the face of modest changes in these parameters. Each source extracted by the software was then identified on a gray scale representation of the field to reject spurious point source identifications such as bright portions of nebulosity.

These procedures were followed for both the frames at H and those at K. Calibration was by comparison with an average of previous photometry of the sources in our survey; by averaging over many sources, we derive a calibration nearly independent of source variability. From this comparison, individual source brightnesses in the survey appear to be accurate to about 15% rms. This relatively low accuracy probably results from a combination of the large pixel scale of these frames and vignetting near the frame edges. However, it is also likely that many of the sources are variable, which would lead us to overestimate photometric errors.

The reduction and calibration of the selected area deep frames was conducted entirely under IRAF, but the general procedures were similar to those described above for the survey. The vignetting in our camera had been removed by the time these frames were obtained, and the photometric accuracy should be 5%–10%.

The aperture photometry was undertaken both to provide greater accuracy than the photometry from the images and to extend the wavelength range to support detailed modeling. It was calibrated by repeated measurements of SR3, which is a standard in the network of Elias et al. (1982). Nonstatistical errors in tracing the measurements to the standard system should be less than 10%.

The resulting source list is provided in Table 1. Sources are designated in the first column by a coordinate-based convention relative to 16^h and $-24°$. The first set of five digits is the minutes, seconds, and decimal seconds of time in right ascension; the second set of four digits is the minutes and seconds of arc in declination. The accuracy of these coordinates is estimated to be about 2'' rms. Objects for which previously existing photometry has been used are indicated in Table 1.

Our photometry and positions agree well with the results compiled by WLY. The only discrepancy is that we do not detect VS 12 at the quoted position; if the positional error for this source is relatively large, it might either lie to the west of the region we surveyed or be identical with GSS 29.

Although we generally confirm the results of Barsony et al. (1989), there are a significant number of discrepancies. We do not detect their sources 11, 34, 35, 41, and 42. Their suggested identification of source 42 with WL 13 would explain our failure to detect it, since WL 13 lies just outside the region we surveyed; however, an error of $\sim 1'.5$ is then required in their position. The tabulated positions in their paper do not agree well with their figure, so we suspect some problem in position determination is responsible for at least some of the undetected sources. Conversely, there are six sources brighter than $m_K = 14$ in our listing and within the region they surveyed but that do not appear in their list: 2417.7−2159, 2418.4−3008, 2420.4−2307, 2420.6−2254, 2422.6−2248, and 2423.0−2256. The lack of complete agreement in the surveys suggests source variability (Barsony et al. observed roughly 1 year before we did). As discussed below, we appear to have detected 2418.4−3008 in a flare; further observations should address this issue for other sources.

The number of sources in our survey as a function of K magnitude is shown in Figure 2; the large increase in source counts below $m_K = 16$ is expected given the detection limit of the frames and results from an increased rate of false source extractions when the ratio of signal to noise is too low. We conclude that the survey is complete to $m_K = 15.5$ and useful in a statistical sense to $m_K = 16$. Similar arguments indicate the survey is complete to $m_H = 17$. All sources extracted at H brighter than this magnitude limit were independently detected on the corresponding frames at K. However, some extremely red sources detected at K were not extracted at H; in these cases, we did manual photometry on the frames around the position of the source to obtain a detection or upper limit at H. All listed sources are based on a minimum of two independent detections, either at both H and K on the original survey, or at

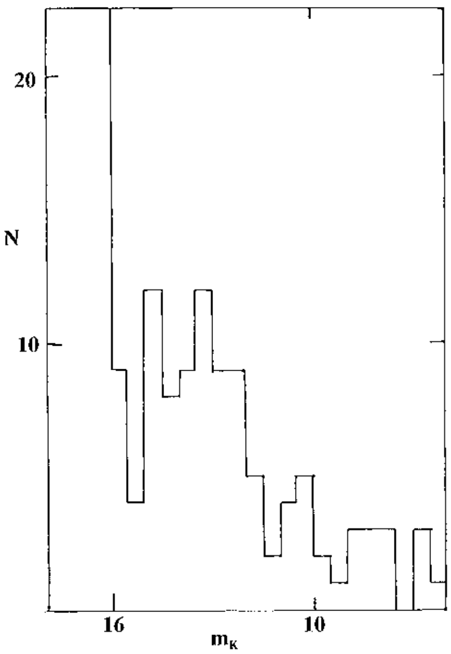

FIG. 2.—Number of sources in our sample as a function of the observed K magnitude.

TABLE 1

INFRARED PHOTOMETRY OF ρ OPHIUCHI CORE SOURCES

Object	J	H	K	L'	M	N	Source
2303.6−1805......	18.8**	15.8	14.2				Ap
2304.5−1657......	16.9	15.3	13.95	12.0**			Ap
2305.4−1241......		>17.4	15.2**				Array[a]
2307.5−1206......		15.9*	12.7	11.0*			Ap
2309.0−1411......	>11.9	10.57	8.95	6.95			VSSG
2310.6−2001......		16.5**	14.9*				Array
2311.0−1554......	>19.1	16.6*	14.1				Ap
2313.3−1421......		>17.6	14.8				Array[b]
		>18.5	16.1*				Ap[b]
2314.4−1237......	14.2	11.6	10.55	9.2			Ap
2315.3−1540......	10.95	9.07	8.10				VSSG
2315.5−1337......		8.7	8.1				El
2315.8−1700......		16.3*	12.7	10.0*			Ap
2316.0−1626......		16.2*	12.6	>11.6			Ap
2317.3−1925......	14.9	13.2	12.0	11.6*			Ap
2317.5−1729......	16.5*	13.85	11.8	10.0			Ap
2317.5−1630......		17.2**	15.0**				Array
2317.6−1622......	16.6*	15.2	12.2	11.6**			Ap
2318.4−1707......		18.1*	16.0*				RR
2318.9−1740......		17.9*	15.7	>12.9			RR
2319.8−1617......		10.49	8.04	6.1	4.4	1.40	El
2320.0−1915......	12.6	11.5	10.9	10.2			Ap
2320.0−1134......		17.7**	15.1**				Array
2320.7−1803......	19.3**	15.8	13.3	12.3**			Ap
2320.8−1708......	15.8	13.6	12.2	11.4*			Ap
2320.8−1721......	16.4	14.8	13.55	12.1*		8.7**	RR
2321.1−1715......		17.0*	15.9*				RR
2321.2−1719......	18.3	15.9	14.5	12.6**			RR
2321.6−1918......	19.2**	16.25	13.85	12.2*			RR
2321.9−1415......		7.63	6.72	5.28			Ch
2322.1−1754......	15.0	12.3	10.2	8.0	6.4	4.8	Ap
2322.3−1143......		15.4*	14.4*				Array
2322.6−1802......	10.52	8.36	7.02				El
2322.8−1233......	>19.2	17.1	14.9	>12.5			RR
2323.8−1640......		17.1	13.1	11.4			Ap
2323.8−1801......	16.55	13.2	11.0	10.0			Ap
2324.1−1619......	17.6*	14.7	13.0	11.7*			Ap
2326.5−1958......	14.1	12.8	12.0	11.5**			Ap
2328.9−1610......		11.97	9.80				VSSG
2330.1−1847......	14.8	12.85	11.7	10.9			Ap
2331.1−1952......	16.7*	14.5	13.2	12.5**			Ap
2332.6−1640......	8.82	7.26	6.29	5.82			El
2339.1−2032......	>18.8	15.9	12.3	10.35			Ap
2341.1−1946......	>19.6	16.5	12.5	11.0			Ap
2341.1−1951......	>19.0	15.6	12.6	11.5			Ap
2346.8−2157......		13.91	10.96	8.7			WL
2349.8−2601......	15.4*	14.7*	14.2*				RR
2350.3−2357......		16.8	13.3	11.6**			Ap
2351.8−2553......	>18.5	16.7	13.0	11.4			Ap
2355.3−2156......	18.2**	14.8	12.8	12.2*			Ap
2355.7−2858......	19.6	15.19	12.78	11.13			WLY
2356.6−3058......		>17.8	14.7*				Array[a]
2357.3−2914......	16.6	13.4	11.8	10.7			Ap
2357.4−2816......		>18.4	14.47	7.8	5.4	3.77	WLY
2400.8−3048......	13.97	10.45	7.82	5.85			WL
2402.6−2146......	16.7	12.65	10.62	8.78		6.2	WLY
2403.7−2948......		>17.9	14.8*				Array[c]
2404.5−2152......	16.8	14.6	13.0	11.8**			Ap
2404.8−3133......		13.8	10.40	7.91			WL
2407.3−2735......	12.59	10.19	8.92	7.9			WL
2407.8−3033......	14.7	10.79	6.78	3.88	2.13	0.63	El
2408.3−2315......	>19.0	16.5	12.8	11.3			Ap
2408.5−2641......		13.82	11.97	10.72		>7.2	WL, WLY
2408.6−2229......	16.8	15.1	14.2	>13.2			RR
2409.5−2807......		13.73	11.71	9.6			WL
2409.7−3149......		14.5	10.71	8.21			WL
2409.8−2611......		17.3	14.5	12.1**			Ap
2412.9−2447......	18.5*	16.5	15.3	>13.2			RR
2413.8−3159......	13.36	10.74	9.28	8.12			WL
2414.0−3159......		12.0*	10.5*				Array
2414.1−2408......	16.6	12.9	10.5				Ap
2416.1−2211......	>16.8	13.99	11.48	8.77		5.6	WLY
2416.6−3234......	19.0**	15.7	12.2	10.3	8.6	6.4	Ap
2416.7−2207......		14.26	10.38	7.92		>7.4	WLY

TABLE 1—*Continued*

Object	J	H	K	L'	M	N	Source
2416.9−2724......		17.3**	15.3**				Array
2417.0−2221......	14.4	11.37	9.59	8.21			WLY
2417.6−3500......	9.54	8.67	8.46	8.22	8.5	>7.1	WLY
2417.7−2159......		14.17	11.2	8.8		6.8	WLY
2418.4−3008......		~13.7	~13.7				Array[d]
			>14.5				Ap[d]
2419.6−3502......	15.7	11.26	8.39	5.88		3.91	WLY
2420.4−2307......		13.94	9.93	7.13			WL
2420.6−2254......		15.2*	13.1*				Array
2422.2−3051......		16.8**	16.5**				Array
2422.6−2248......	>19.3	15.1	12.2	11.1		7.8	Ap
2422.6−3507......	18.3**	15.3	12.6	11.4			Ap
2422.8−3423......	>19.1	17.3	13.0	9.7			Ap
2423.0−2256......	>18.4	15.0	12.4	11.2*			Ap
2424.5−3759......	>18.4	15.7	13.4	>12.0			Ap
2424.7−3245......	16.0	12.35	9.8	8.4	7.7	7.1	Ap
2425.1−3410......		13.61	9.96	6.85		3.34	WLY
2431.3−3435......	11.8	9.2	7.8	6.6			Ap
2431.5−3354......		17.7**	15.0**				Array

[a] The reality of this source was confirmed with the aperture photometer under nonphotometric conditions.

[b] Based on the two measurements listed and a third obtained under nonphotometric conditions, this source appears to have dimmed substantially between 1989 May and 1991 April.

[c] Although we have only detected this source once, its reality is confirmed by a radio identification.

[d] This source appeared to vary during the course of our measurements in 1989 May, and dimmed substantially by 1991 April.

SOURCES.—*Ap:* Aperture photometry from the Multiple Mirror Telescope. In these cases, data with nominal errors of 10% or less are unmarked, errors of $\simeq$20% are indicated with an asterisk, and errors of 30%–40% with two asterisks. *Array:* CCD array photometry from the Steward Observatory 90 inch (2.3 m) telescope. Errors are indicated as for the MMT photometry. *WL:* Wilking & Lada 1983. *VSSG:* Vrba et al. 1975. *El:* Elias 1978a. *Ch:* Chini 1981. *WLY:* Wilking, Lada, & Young 1989. *RR:* Rieke & Rieke 1990. Errors are indicated as for the MMT photometry reported for this paper.

K with follow-up aperture photometry (in a few cases, the confirmation was under nonphotometric conditions so the photometry is not entered in the table), or at K with an identification in the radio survey of Leous et al. (1989).

An experiment was devised to test the reliability of the survey. Frames were extracted for one-eighth of the total integration time for a portion of the survey in which there was a high density of faint sources. The reduction in signal-to-noise ratio for these frames should be 1.1 mag, and the full survey data for the same positions could be used as a "truth test" of the data reduction with this reduced sensitivity. The frames were analyzed using identical procedures as for the survey. All sources with $m_K < 14.8$ were identified, while some sources began to be missed at $m_K > 15$. This behavior is exactly as would be expected given the sensitivity limits quoted above and substantially increases our confidence that the survey is complete to $m_K \simeq 15.5$.

A second test is based on our limited area deep frames, which detected 15 sources; the faintest objects were at $m_K =$ 17.5 to 18. Seven of these sources were brighter than $m_K = 15.5$, and all seven appear in the original survey. Two new sources were detected at $m_K = 15.7$ and the remaining six sources were at $m_K > 16.2$. Again, these results are as expected, although they suggest significant incompleteness below $m_K = 15.5$.

4. ANALYSIS

To interpret these data, it is necessary to relate them to physical properties of the detected objects. Since only photometric observations are available, the source luminosities are the most directly constrained parameters. Below, we describe how luminosities were estimated. Section 4.1 reviews the theoretical foundation of our analysis. We include a study of the uncertainties in the models of substellar objects, since our luminosity estimation is heavily dependent on these models. Section 4.2.1 discusses the extinction law, which is critical to interpreting these objects. In § 4.2.2, we analyze the commonly used calorimetric method for deriving luminosities and determine its regime of applicability, showing that it cannot be expected to give valid results for heavily reddened low mass objects such as many of the sources in our survey. In § 4.2.3, we develop a new method of luminosity estimation particularly applicable to low-mass ($M < M_{\odot}$) objects; in § 4.2.4, we describe the results of a variety of tests of this technique. In § 4.2.5, we discuss how luminosities were estimated for the sources which may still be actively accreting material.

4.1. *Properties of Low-Mass Young Stellar Objects*

4.1.1. *Spectral Energy Distributions*

The spectral energy distributions of young stellar objects have been discussed extensively by Adams et al. (1987). They characterize the near and mid infrared fluxes f_λ emitted by an object by means of its spectral index n defined as

$$n = \frac{d \log (\lambda f_\lambda)}{d \log \lambda} . \quad (1)$$

Different spectral indices observed in star forming regions are interpreted as an evolutionary sequence, where objects with

$n > 0$ (class I) are the accreting envelopes infalling on central, hidden protostars. Objects with $0 > n > -2$ are T Tauri stars (class II), still surrounded by a nebular disk responsible for their infrared excesses. When this disk further disappears, the observed continuum spectral energy distribution can be fitted well by that of a reddened blackbody (class III), with $n \simeq -3$ at long wavelengths.

Low-mass class III objects are therefore modeled as blackbodies with appropriate corrections for the effects of absorption features that occur in the photometric bands. For low-mass class II objects, the results of Adams et al. (1987) show that the shape of the emergent energy distribution at visible and near-infrared wavelengths can be approximated by that of a blackbody, up to the wavelength where $d \log (\lambda f_\lambda)/d \log \lambda$ has its maximum, that is, up to

$$\lambda_m = \frac{T_P}{T_*}, \quad (2)$$

where $T_P = 3671$ K μm and T_* is the effective temperature of the central star. Up to λ_m, our models are similar to those for class III. The flux at longer wavelengths shows the infrared excess attributed to the circumstellar dust and characterized by the index n. We have modeled the infrared excess in a quantitative way which matches to an acceptable degree of accuracy the results of Adams et al. (1987). The spectral index defined by equation (1) may be written in terms of the dereddened magnitude m_λ as

$$n = -0.4 \frac{dm_\lambda}{d \log \lambda} - 3, \quad (3)$$

where we have used the fact that, at long wavelengths, the flux from a zero-magnitude star decreases as λ^{-4}. The magnitude difference between a class II and a class III object at long wavelengths is then

$$\Delta m_\lambda = C - 2.5(n + 3) \log \lambda . \quad (4)$$

For our model class II stars, we assume expression (4) to hold for all the wavelengths longward of λ_m, with $\Delta m_{\lambda_m} = 0$; thus,

$$\Delta m_\lambda = 2.5(n + 3) \log \frac{T_P}{\lambda T_*} . \quad (5)$$

The spectral energy distribution of class I objects in the near-IR is characterized by a steep rise of the flux with increasing wavelength, with some broad superposed absorption bands due to water ice and silicates. The luminosities are due to the release of potential energy of the infalling material, and only rough approximations to the physical parameters of the embedded objects are possible.

4.1.2. *Stellar Models*

Models of low-mass stars covering the early stages of evolution have been published by D'Antona & Mazzitelli (1985) and Nelson, Rappaport, & Joss (1986); later stages are modeled by Burrows et al. (1989). The agreement of these models in their different overlapping regions is reasonably good, and we have chosen the D'Antona & Mazzitelli ones to have a homogeneously calculated grid including a relatively wide span of masses. An improved set of models is in preparation by Burrows et al. (1992). A preliminary comparison of this new work with that of D'Antona & Mazzitelli shows the older models to underestimate the source luminosities systematically by a factor of roughly 1.5, but otherwise to show similar trends if tracks of similar luminosity are compared. Therefore, although the new models were not available in time for our analysis, the results would not have changed significantly except that the new models would have led to slightly lower mass estimates.

The evolutionary state of the low-mass stars in the ρ Ophiuchi region can be estimated in several ways. Various lines of evidence indicate that the region is not older than 3.5×10^6 yr (see WLY and references therein), and observational results suggest that the T Tauri stars are significantly younger, with a maximum age around 1.5×10^6 yr. To place our observed stars on a given isochrone from the theoretical models, we have assumed 8×10^5 yr and 2×10^6 yr as the approximate ages for our stars when considering them as class II or class III objects, respectively. We have confirmed that our fits are insensitive to variations in these parameters. On the other hand, the relative numbers of different classes of objects derived in our analysis should allow us to check for the consistency of the initially assumed ages.

It is noteworthy that low-mass ($M < 0.1$ $M_\odot$) objects undergo deuterium burning over the 2×10^6–5×10^6 yr stage of their evolution. As a result, their luminosities and temperatures are relatively stable during this phase. Consequently, for low-mass objects our analysis is not sensitive to particular assumptions about the distribution in ages.

The form of the luminosity-temperature relationship is particularly important for our analysis. For high- and intermediate-mass stars, it can be represented by a power law of the form

$$L \propto T^\beta , \quad (6)$$

where β is determined locally for different mass ranges. Because of the short time spent by stars with $M > 3\,M_\odot$ on the pre–main-sequence stage, we can safely assume that nearly all the stars in this mass range are in or near the main sequence, where $\beta \sim 5$. Intermediate-mass stars with $M \simeq 1$–3 $M_\odot$ are developing a radiative core at the age of the ρ Ophiuchi cluster, which progressively increases the surface temperature while the star is still contracting (Iben 1965). On a given isochrone, stars toward the top of this mass range are significantly closer to the main sequence than those near the bottom, thus being smaller and hotter. The decrease in radius and increase in surface temperature as we proceed on the isochrone toward higher masses in this interval gives an exponent $\beta \sim 3$ in the power law (6). Low-mass stars have fully convective interiors (Stevenson 1991), and on their way toward the lower end of the main sequence their luminosities decrease with only a slight increase of temperature. Thus, for stars in our sample with $M < 1\,M_\odot$ and on a given isochrone, the temperature is roughly independent of the luminosity.

4.1.3. *Uncertainties in the Models*

Although the available models (D'Antona & Mazzitelli 1985; Nelson et al. 1986; Burrows et al. 1989, hereafter BHL; Burrows et al. 1993, hereafter BHSL) of low mass stellar and substellar objects appear to be in reasonably good agreement, there is a suspicion (e.g., Stevenson 1991) that large uncertainties still exist at the age of the ρ Oph cluster. This question will be examined in detail by BHSL. Because of its importance to the work reported here, however, we discuss it briefly.

At extremely young ages (<100,000 yr), variations in the conditions of formation affect the state of low-mass objects.

However, at the appropriate masses and ages for ρ Oph, these initial transients have died out in the models. The primary remaining candidates for uncertainty are discussed below.

To investigate the range of effective temperatures ($T_{\rm eff}$) and luminosities (L) that would be reasonable within the uncertainties of current theoretical models, we employ the results of BHL and BHSL. These authors have generated evolutionary tracks for objects between 0.01 and 0.2 $M_\odot$, between ages of 10^5 and 2×10^{10} yr, and for a variety of metallicities (Z), mixing lengths, assumptions concerning opacities, and deuterium (Y_d) and helium (Y_α) abundances. For the purposes of this discussion, we will focus on a brown dwarf at 0.07 $M_\odot$ and at the age of the ρ Oph cluster. It should be remembered that the various parameter dependences can be different in other regions of mass-age space. However, we believe our conclusions about the theoretical terrain that can be occupied by a 0.07 $M_\odot$ brown dwarf at the age of ρ Oph are robust and are in fact representative of the parameter dependences throughout the entire brown dwarf family.

The equation-of-state dependence is minimal, as can be seen by comparison of the work of Saumon & Chabrier (1991) and Marley & Hubbard (1988). The only major questions that remain regarding the equation of state concern the phase transition from molecules to metal; at the age of ρ Oph, little of a brown dwarf's mass is at the requisite densities ($\rho > 1$ gm cm^{-3}) for these concerns to be significant. This statement is particularly true of the heavier brown dwarfs.

With the equation of state well in hand, we turn to the dependences on Y_α, mixing length, Y_d, and Z. The first two, Y_α and mixing length, introduce only small ambiguities. For our canonical 0.07 $M_\odot$ brown dwarf at the age of ρ Oph, $T_{\rm eff}$ and L change by <40 K and 10% respectively for Y_α's between 0.22 and 0.28; $T_{\rm eff}$ and L change by <200 K and 10% respectively for mixing lengths between H_p and 1.6 H_p, where H_p is the pressure scale height.

However, the Z-dependences can be large. For instance, our 0.07 $M_\odot$ ρ Oph brown dwarf would be hotter by 1060 K and less luminous by 40% if it had $Z = 0$ rather than solar metallicity (the radius achieved by the $Z = 0$ dwarf at 3×10^6 yr is 2 times smaller than the radius of a solar abundance dwarf). While zero metallicity is extreme and represents Population III or extreme Population II subdwarfs, the above comparison serves to illustrate the importance of determining the metallicity to assess a population of objects adequately. Assigning a more reasonable range of uncertainty to the metallicity, from the work of BHL and BHSL we surmise an ambiguity in $T_{\rm eff}$ of no more than 300 K and in L of less than 15% for our 0.07 $M_\odot$ dwarf. Interesting complications in opacity calculations arise when grains form in an atmosphere. However, for solar metallicity brown dwarfs above a mass of 0.02 $M_\odot$ and at the age of ρ Oph, $T_{\rm eff}$ is above 2700 K and grains do not form in the photosphere. At the temperatures of interest for our modeling, the emergent spectrum should be similar to that from normal M dwarf stars.

The dependence on Y_d can also be important. Y_d is thought to lie near 2×10^{-5} (McCullough 1992); we have evaluated the effect of an overabundance by a factor of 2.5 to a level of 5×10^{-5}. Since a brown dwarf above a mass of 0.015 $M_\odot$ is in or around its deuterium-burning phase at the age of ρ Oph, such an object's properties are dependent on Y_d in interesting ways. For instance, if Y_d is increased from 2×10^{-5} to 5×10^{-5}, $T_{\rm eff}$ decreases by only about 70 K for a ρ Oph dwarf at 0.07 $M_\odot$, but the luminosity increases by about 40%.

In summary, we conclude that $T_{\rm eff}$ for models of young low-mass stars and brown dwarfs has a significance dependence on Z and L has one on Y_d. Ambiguities in the comparison between observation and theory depend more strongly on the measurable physical inputs Z and Y_d than they do on the theoretical arcana. Allowing for the largest plausible uncertainties in these quantities, the uncertainties in the models are of the order of 300 K in $T_{\rm eff}$ and 40% in L. We have verified that our conclusions are not dependent on the models to this degree of accuracy (see § 4.2.3). In fact, the models we have selected for our analysis appear to underestimate the luminosities compared with the work by BHSL and by a factor comparable to the largest uncertainties in the models. Hence, our estimated masses are the maximum values consistent with the more recent models within possible systematic modeling uncertainties.

4.2. *Determination of Luminosities*

4.2.1. *The Extinction Law*

Because the sources in our survey are heavily obscured, determining their natures requires knowledge of the near infrared extinction law. In the visible, there is evidence for anomalous extinction in this region, with $R = A_V/E_{B-V} \gg 3$. For example, the study of extinction by Rieke & Lebofsky (1985) includes o Sco, which lies only 3° away from the ρ Oph cloud and has $R = 4$. However, the infrared extinction law to this star was found to be indistinguishable from that in other directions. In addition, Harris, Woolf, & Rieke (1978) found the Ophiuchus extinction law to deviate only subtly from the average law even if all observed deviations were ascribed to the extinction law and not to properties of the embedded sources such as infrared excesses. We have therefore used the apparently universal near-infrared extinction law as derived by Rieke & Lebofsky (1985) and Clayton & Mathis (1988). We demonstrate in § 5.2 that use of an extinction law with shallower wavelength dependence, as has been suggested applies to this region, is incompatible with our data.

4.2.2. *The Calorimetric Method*

Most attempts to determine the luminosities of dust embedded young stellar objects use calorimetric methods (WLY; Kenyon et al. 1990; Beichman et al. 1992), based on the luminosity represented by the observed fluxes with an extrapolation to the longer wavelengths on the basis of a number of physical assumptions regarding the spectral energy distributions of the sources outside the observed range. As pointed out by WLY, the accuracy with which it is possible to determine the bolometric luminosity from this method depends on the extinction being entirely produced by a dust shell which surrounds the source and reradiates the absorbed energy into the measurement beam at infrared wavelengths.

For low-luminosity, relatively cool objects, the distance the short-wavelength radiation travels before being absorbed and the low frequencies at which it is reradiated make it unlikely that the reemitted long-wavelength radiation will be recovered in the available measurements. A simple model of the influence of the common surrounding medium for a typical embedded class III source in ρ Ophiuchi can be useful to understand the limitations of the calorimetric approach. Let us assume that a star is embedded in the center of the cloud, taken to be spherical and homogeneous, with an extinction $a_V = 25$ mag pc^{-1}. The radius of the cloud is approximately 1 pc, and the cloud is assumed to be transparent to the infrared radiation reemitted by the grains. We will neglect scattering by the dust grains and will assume that they have characteristic absorption efficiencies $Q_{abs}(\lambda)$. For this simple illustration, we assume that $Q_{abs}(\lambda)$ is proportional to the extinction.

With these assumptions, it is straightforward to compute both the spectral energy distribution and the distribution on the sky of the emergent flux from the embedded star, assuming that the grains are in thermal equilibrium. In Table 2 we give the fraction of the total luminosity of the central star that is recovered in the form of dust emission up to a certain wavelength and compare this fraction with what would be recovered up to the same wavelength but using a beam 30″ in diameter. For low-luminosity, low-temperature objects, particularly where measurements are only available to 10 or 20 μm, only a small portion of the emergent flux is recovered. Even where longer wavelength data are available, only a small fraction of the total luminosity would be captured by a beam of reasonable size; in crowded regions like ρ Oph, it would be impossible to identify the contribution of a single source. The situation is more favorable for luminous, hot objects since their outputs are peaked toward wavelengths <100 μm and *IRAS* measurements allow recovery of the majority of their emission.

Calorimetric measurements of objects embedded in the ρ Ophiuchi cloud can severely underestimate their luminosities unless they are very hot and the contributions from long wavelengths are considered.

4.2.3. *Luminosities of Class II and Class III Objects*

Since for cool, low-luminosity objects in the ρ Ophiuchi cloud we cannot measure most of the luminosity that is absorbed and reemitted by the dust grains in the far-infrared, we are forced to reconstruct the original spectral energy distribution of the unreddened object. We did so for each object by assigning an age from the spectral properties, assuming a mass, and determining a hypothetical luminosity and temperature from the theoretical isochrones. The reddening was adjusted to give an optimum fit to the observed magnitudes of this hypothetical object. The procedure was repeated for other input masses until mutually consistent estimates of the luminosity, temperature, and reddening were obtained.

The details of this fitting procedure were as follows. For a given temperature T, the star can be parametrized by a Rayleigh-Jeans magnitude, M_{RJ}, defined as the absolute magnitude that a blackbody would have at wavelengths corresponding to the Rayleigh-Jeans part of the spectrum. It can be shown that this magnitude is related to the infrared luminosity of the star longward of a certain λ_1 lying on the Rayleigh-Jeans tail of the Planck function:

$$\lambda_1^3 L_{IR} = 14.04 \times 10^{-M_{RJ}/2.5}\ L_\odot\ \mu\text{m}^3\ . \tag{7}$$

TABLE 2

RECOVERED FRACTION OF THE LUMINOSITY OF A STAR IN THE CLOUD

T(K)	Up to 10 μm	Up to 25 μm	Up to 100 μm
20,000......	0.06 (0.06)	0.53 (0.37)	0.96 (0.46)
15,000......	0.02 (0.02)	0.26 (0.20)	0.54 (0.27)
10,000......	0.01 (0.01)	0.06 (0.06)	0.22 (0.13)
6000......	0.01 (0.01)	0.02 (0.02)	0.12 (0.06)
3500......	0.04 (0.04)	0.04 (0.04)	0.12 (0.06)
2700......	0.08 (0.08)	0.08 (0.08)	0.15 (0.09)

NOTE.—Values in parentheses are the fractions recovered within a beam of 30″ in diameter centered on the position of the star.

The product $\lambda_1^3 L_{IR}$ is related to the temperature and bolometric luminosity L of the star by

$$\lambda_1^3 L_{IR} = \frac{2\pi}{3} \frac{kc}{\sigma} \frac{L}{T^3}, \tag{8}$$

so that we finally obtain

$$\frac{L}{T^3} = 9.17 \times 10^{-11} \times 10^{-M_{RJ}/2.5}\ L_\odot\ \text{K}^{-3}\ . \tag{9}$$

The fitting procedure we have adopted for class II and class III objects consists of assuming a temperature and a spectral index for the star and calculating the differences $c_\lambda^1(T)$ between the absolute magnitude of the star in each wavelength and M_{RJ} due to the fact that blackbody spectra for the effective temperatures in our measured wavelength range are not Rayleigh-Jeans either for the embedded stars or for the A stars which set the magnitude scale zero point. Another correction $c_\lambda^2(T)$ is added to the J, H, and L' magnitudes due to the temperature dependent absorption features affecting the fluxes at these wavelengths. These corrections were estimated from stellar atmosphere models by Allard (1990) for a star with $\log g = 5.0$ and solar metallicity. Finally, if the unreddened spectral index is taken to be $n > -3$, a third correction $c_\lambda^3(T)$ is added for filters having λ larger than the one given by equation (2), $c_\lambda^3(T)$ being given by equation (5).

The addition of all the temperature dependent corrections, summarized by $c_\lambda(T) = c_\lambda^1(T) + c_\lambda^2(T) + c_\lambda^3(T)$, is inserted in a system of linear equations to find the best fitting Rayleigh-Jeans magnitude M_{RJ} and the extinction A_V toward the star:

$$m_\lambda + D + c_\lambda(T) = M_{RJ} + \alpha_\lambda A_V\ , \tag{10}$$

where α_λ is the wavelength dependence of the extinction. We have an equation (10) for each measured magnitude m_λ at the wavlength λ. D is the distance modulus to the stars, assumed to be known. The system of equations (10) is solved by least squares. Due to the potentially significant contribution by thermal reradiation from the dust at 10 μm, only the J, H, K, L' (and M when available) measurements are used in solving the system (10).

The solution of system (10) gives us the Rayleigh-Jeans magnitude M_{RJ} and the extinction A_V for a given assumed value of the temperature. By means of equation (9) we then check if this temperature and luminosity are consistent with evolutionary models for young stellar objects, and the temperature is iterated until consistency is obtained.

As we saw in § 4.1.2, stars in the range 1–3 $M_\odot$ with a growing radiative core show an approximately constant L/T^3 relationship. Furthermore, the temperature-dependent corrections included in $c_\lambda(T)$ tend to decrease and lose sensitivity to temperature at infrared wavelengths as the star gets hotter. As a consequence, the intermediate-mass stars are expected to appear in our sample as a clump of similar Rayleigh-Jeans magnitudes M_{RJ} and quotients L/T^3, but for which temperature and luminosity cannot be separately estimated. Thus our method of luminosity estimation in the ρ Ophiuchi cloud is restricted to stars with subsolar mass contracting towards the main sequence or to massive stars ($M > 3\ M_\odot$) having already reached the main sequence.

4.2.4. *Tests of the Luminosity Estimation*

We tested the reliability of our method of luminosity estimation for low-mass stars in a variety of ways. First, we generated artificial data for stars with foreground extinctions ranging from $A_V = 5$ to $A_V = 70$ mag, and with photospheric temperatures ranging from 2800 to 4000 K. Luminosities were assigned according to the calculations of D'Antona & Mazzitelli (1985) using effective temperatures as input parameters. Next, the expected apparent magnitude in each band was calculated by inverting the procedure described in § 4.2.3, and random noise with an amplitude of 0.2 was added to that magnitude to simulate errors in the measurements.

Our method was then applied to the set of artificial stars to investigate the sensitivity of the derived stellar parameters to measurement errors. For the colder stars ($T < 3000$ K), only large measurement errors can change the derived temperature by a significant amount; with the quoted levels of random noise, the recovered temperature lies always within 20 K of the input value. Given the steepness of the temperature-luminosity relation for cool objects, the recovered luminosity can differ as much as 15% from the input value, while the derived mass falls within 10% of the input. The extinction remains remarkably close to the original value, within $\delta A_V = 2$.

For hotter stars ($T > 3000$ K), the errors in derived temperature increase and can reach 50 K at $T = 3500$ K. Nevertheless, the relatively milder dependence in this region of both luminosity and mass on temperature keep their errors close to the range quoted above, as is also true of the extinction. Occasionally, when the random noise makes the reddest magnitudes significantly brighter, we obtain lower temperatures and extinctions and a flatter spectral index, thus mimicking an intrinsic infrared excess. In such cases, both luminosity and mass can be underestimated by up to 25% and the spectral index can be increased a few tenths. The conclusion of these experiments with artifically generated data is that measurement errors should not be an important source of error in our analysis.

Next, to test the sensitivity of our method to the existence of reradiating circumstellar dust, we added to our artificial stars several blackbody excesses of different temperatures and luminosities. Although circumstellar reradiation can have a variety of spectral energy distributions in the mid-infrared, the sublimation of dust at about 1500 K and the relatively short wavelengths used in our fitting will result in our test cases being broadly representative. In Table 3, we show the recovered parameters, which demonstrate that, in general, reradiating circumstellar dust has little influence. It can be seen that the primary effect of a cool, moderately luminous added blackbody is to increase the recovered spectral index, as may be expected from the existence of an infrared excess, but with little influence on the recovered luminosity of the star. This can be understood in terms of our method being primarily sensitive to the stellar luminosity and only secondarily to the colors, and to the fact that our observational data are at wavelengths where the reradiated emission is relatively weak compared to the photospheric emission. The addition of a blackbody with similar temperature and luminosity as those of the central star approximately reproduces the effects of a binary pair, and indeed we obtain a luminosity approximately twice that of the central star. On the other hand, our method fails in reproducing the input parameters in the situation of the added blackbody being roughly 5 times cooler but with a luminosity comparable to that of the central star. As the temperature of the additional component drops below this level, its effects will become negligible given the wavelengths at which we do the model fitting.

TABLE 3

REPRODUCED PARAMETERS OF AN ARTIFICIAL STAR PLUS A BLACKBODY

T_{bb} (K)	L_{bb}/L_*	A_V	L_*	n
......	0	18	0.09	−3.0
500......	0.3	18	0.08	−2.7
1500......	0.3	18	0.10	−2.4
2500......	0.3	19	0.14	−3.0
500......	0.6	15	0.04	−2.0
1500......	0.6	18	0.10	−1.9
2500......	0.6	20	0.20	−3.0
500......	0.9	14	0.03	−1.5
1500......	0.9	18	0.11	−1.7
2500......	0.9	20	0.26	−3.0

NOTE.—The central star has an effective temperature of 3000 K and a luminosity of 0.1 $L_\odot$ and is obscured by $A_V = 18$. T_{bb} is the temperature of the added blackbody and L_{bb}/L_* its luminosity as a fraction of the star luminosity. A_V, L_*, and n are the recovered values of the extinction, the luminosity, and the spectral index of the artificial star, respectively.

We also explored the consequences of choosing different isochrones for the fitting of our data. The primary effect of a large increase in the assumed age of a star is to increase the mass derived through the theoretical models; however, we found that this mass increase is negligible within the age ranges to be expected in the ρ Ophiuchi cluster (i.e., up to 10^7 yr). The insensitivity to age for the very low mass objects arises because deuterium burning is effective in stabilizing the output over the range of ages that is plausible for this cluster. For the substellar objects indicated by our analysis, the luminosity decreases by about a factor of 3 with little change in temperature between ages of 2×10^6 and 10^7 yr. Objects for which we deduce masses of 0.04 $M_\odot$ or less would still be fitted as substellar at an age of 10^7 yr.

We have examined the effects on our luminosity estimates caused by the dominant sources of uncertainty in the theoretical models of low-mass objects as we have summarized them in § 4.1.3. First, we considered the possible 40% luminosity increase for objects of a given mass that would accompany a deuterium overabundance of a factor of 2.5. We found that our luminosity estimation was virtually unaffected because, in the low-mass region, the luminosity/temperature relationship is very steep. As a result, our procedure would reduce the temperature slightly and return a source with similar colors, luminosity, and extinction to the previous estimates. Second, we evaluated the effects of uncertainties in metallicity that might change the temperatures of the objects by 300 K. The worst case was found to be for a temperature increase by this amount. For substellar and low-mass stellar objects, it resulted in an increase in the estimated source luminosity by about 10%. For objects just under 1 $M_\odot$, an increase by about 20% was observed.

The source 2417.6−3500 is the single instance of a low-luminosity object where spectroscopic data are available to compare with our classification; as noted after Table 4, the agreement is good. As an additional test, we fitted three late-type spectroscopically classified sources in Taurus-Auriga (Kenyon et al. 1990). These fits are very approximate because we did not adjust the source ages from the fits for ρ Oph. Nonetheless, reasonable results were obtained: 04298+2246 was found to be similar to Oph 2417.6−3500 but of slightly higher luminosity and mass (spectra are also similar), and 04185+2022E and W are deduced to have luminosities of about 0.1 $L_\odot$ and masses of about 0.2 $M_\odot$.

4.2.5. *Luminosities of Class I Objects*

Objects in an active accretion phase (i.e., those of class I) cannot be fitted by our scheme. Usually, they can be recognized as very red objects from their $H-K$ color indices, with lower $K-L'$ indices (possibly due to the water ice absorption feature near $\lambda = 3.1$ μm which reduces the flux in L'). In addition, the possible protostellar objects usually show very large mean residuals when we try to fit them as class II or class III objects, regardless of the derived value of the extinction. Thus, we have used these observational criteria to identify possible class I objects appearing in our lists.

The luminosity of protostellar objects is largely determined by the accretion rate, rather than by the physical parameters of the embedded source, and only very rough estimates of the physical parameters are possible. To obtain estimates of the luminosities, we first assume a representative value of the spectral index for our objects. Then, by using observed magnitudes instead of fluxes in equation (1), the following relation is obtained:

$$m_\lambda - 2.5(n+3)\log\lambda = C + \alpha_\lambda A_V\,, \tag{11}$$

where C is a constant independent of wavelength. An equation (11) can be written down for each measured magnitude m_λ (including the *IRAS* fluxes where available), and the least-squares solution of the resulting system of equations gives us the value of the extinction under the input assumptions.

We can then deduce the fluxes in each wavelength that would be observed in the absence of extinction, f_λ. An appropriate power law for f_λ is defined by equation (1). By numerically integrating over the observed wavelength range, we obtain an integrated infrared flux, $\mathscr{F}_{\rm IR}$. The total integrated flux is found by assuming, as did WLY, that the spectral energy distribution has a slope n from $\lambda = 0$ μm to $\lambda = 100$ μm and decreases with $n = -1$ thereafter. Our luminosity estimate is then

$$L = 4\pi d^2 \mathscr{F}_{\rm tot} = 4\pi d^2 \frac{(n+1)\mathscr{F}_{\rm IR}(100\ \mu{\rm m})^n}{\lambda_2^n - \lambda_1^n}\,, \tag{12}$$

where d is the distance to ρ Ophiuchi. Obviously, equation (12) gives only a very rough approximation with observations only at near-infrared wavelengths, and calorimetric estimates may be more accurate if mid-infrared data are available.

5. RESULTS AND DISCUSSION

The results of our modeling of the ρ Ophiuchi population of stars are summarized in Tables 4 through 9. The extinctions we have derived for these sources are generally <50 mag; since we surveyed within the region where the total $A_V > 50$, this result is consistent with our initial assumption that the sources are embedded at various depths in the cloud, although the clumpy distribution of absorbing material in the cloud (Loren 1989) must also influence the analysis. The discussion of this embedded population begins with a consideration of the degree of contamination of the sample in § 5.1 and then provides details regarding the low-mass (§ 5.2), high-mass (§ 5.3), intermediate-mass (§ 5.4), and class I (§ 5.5) objects. Following the discussion of individual objects, in § 5.6 we show how we make completeness corrections to derive the underlying population in the forming cluster, and in § 5.7 we use the expected age distribution of objects to test our modeling. Finally, in § 5.8, we derive the luminosity and mass functions for the cluster.

5.1. *Possible Nonmembers of the ρ Ophiuchi Population*

The sensitivity of our survey makes it possible to detect either faint, old main-sequence foreground stars or bright, heavily reddened background stars. However, statistical arguments can be used to estimate some limits on the contamination by nonmember sources in our results.

Foreground main-sequence stars should be distinguished by their blue colors, and the expected number in our sample can be deduced from the number of stars in the solar neighborhood (Mihalas & Binney 1981). The result is that only about two such stars should lie within the solid angle subtended by the surveyed area. Actually, one of the stars in our sample, 2422.2−3051, is a little reddened, faint object. An approximate fit (this object has only two low weight colors) would make it a low-luminosity main-sequence M dwarf that lies in front of the ρ Ophiuchi cloud. Rieke & Rieke (1990) suggest that 2349.8−2601 may be a foreground star on the basis of its relatively blue colors. Although the luminosity of this star is consistent with its being a member of the embedded young population, it is also possible that it is a foreground object just in front of the obscuring cloud. We consider both these objects to be likely foreground stars, and they will not be included in our further discussion. From the density of stars in the solar neighborhood, it is easy to show that the probability that a field interloper lies within the cloud is negligibly low.

Background stars may be more difficult to distinguish from intrinsically very red objects, mainly class I, embedded in the ρ Ophiuchi cloud. Red giants and supergiants are the most likely background sources within the detection level of our survey, main-sequence stars being too faint at K to be included. Assuming a typical extinction of $A_V = 70$ mag for the background stars and typical $V-K$ color indices for red giants, the faintest apparent V magnitude without extinction for a star to be included in our K-magnitude–limited survey would be around 12.8. The total number of stars brighter than a given magnitude has been tabulated by Bahcall & Soneira (1980) as a function of Galactic longitude and latitude. For the direction of ρ Ophiuchi, we may expect about 100 stars brighter than $V = 12.8$ per square degree in the absence of the cloud. In the area covered by our survey, this gives a number of background stars of about five. The counts of background stars per magnitude interval should rise by a factor of ~ 2.75 per magnitude; i.e., there should be ~ 3.2 15th mag background stars, ~ 1.2 14th mag ones, and ~ 0.7 brighter than 14th mag.

To identify the possible background stars, we have assumed the sources in our sample to be supergiants (to obtain an upper limit to the distance) with a luminosity $L = 3 \times 10^4\ L_\odot$ and have calculated their expected absolute magnitudes for different values of the temperature. By fitting to the observed magnitudes, we have then derived the extinction A_V and the distance modulus D under these assumptions and have regarded the stars for which we get a good fit with $A_V > 50$ mag and $D > 6.1$ as possible background stars. A total of 14 stars meet these requirements, a factor of 3 above the expected number of background stars. However, we can eliminate most of them because after dereddening they are excessively bright for background objects (e.g., $m_K \sim 6$), because they display characteristic activity of young stellar objects (e.g., radio emission or variability), or because they are better fitted by other possibilities. Finally, we are left with only three objects which may be background luminous stars: 2404.8−3133 = WL 17, 2409.7−3149 = WL 19, and 2420.4−2307 = WL 6. It is extremely unlikely that all three objects are background stars, on the basis of the predicted number of background stars of that magnitude ($K < 11$) per square degree, and the most likely alternative is that they are class I objects belonging to the ρ Ophiuchi population. Four fainter stars, 2311.0−1554, 2316.0−1626, 2356.6−3058, and 2403.7−2948, may be background stars, but the lack of measurements in wavelengths other than H and K makes this assignment uncertain. Thus, the number of our candidate background stars is likely to be less than seven, well in agreement with the statistically expected result of five.

A direct estimate of the number of background stars can be obtained from the survey of a nearby background region by Greene & Young (1992). Where we would estimate 45 background stars brighter than $K = 14$ from the model of Bahcall & Soneira (1980), Greene & Young find 30. As a result, it is unlikely that our use of the Bahcall & Soneira models underestimates the expected number of background stars.

The number of background stars in our survey at a given brightness limit will increase relative to these estimates if the extinction is patchy and there is significant area with a lower column of interstellar material which is counterbalanced by areas with a higher column. Because the extinction is estimated from CO maps with a 1:1 beam (Wilking & Lada 1983), patchiness on a small spatial scale would be undetected.

We used the deep images of 15 arcmin^2 to examine the issue of patchy extinction and background contamination in more detail. These images reach $m_K = 17.5$–18 and $m_H = 18.5$–19, 2–2.5 mag fainter than the whole survey. Assuming a uniform extinction level of $A_V = 70$ mag, we would predict 5.4 background stars with $18 > m_K > 15.5$ in this survey. The number of background stars would be significantly larger than this estimate if the extinction were patchy. The total number of objects detected in this magnitude range is 8; all are quite red in $H-K$ (most are not detected at H). Some of the faint detections are likely to be embedded in the far side of the ρ Oph cloud, so this experiment supports our estimates based on the Bahcall & Soneira model and an assumption that reasonably uniform, heavy extinction associated with the cloud blocks out most of the background.

5.2. *Low-Mass Objects*

Our survey reveals the existence of a number of faint, relatively blue objects which can be regarded as likely low-mass stars, and some fulfill the requirements to be considered as candidate substellar objects. In Table 4, we give the deduced parameters for sources giving a good fit when assumed to belong to this group, with magnitudes measured in three or more filters, for which in principle extinction and spectral index can be calculated and an estimation of the physical parameters is possible. Objects with a mean residual larger than 0.2 mag have been excluded. One source, 2355.3−2156, is probably low in mass because it is faint, but we had difficulty obtaining a satisfactory fit for any class of object.

Some of the brightest objects in Table 4 were studied by WLY, who could make some estimates of their luminosities from calorimetric measurements. Our estimates of luminosities are consistent with the upper limits set by them for three of the objects: 2355.7−2858 = WL 21, 2357.3−2914 = WL 14, and 2409.5−2807 = WL 11. For 2408.5−2641 = WL 9, we find a luminosity clearly above the upper limit given by WLY; however, we may attribute this discrepancy to the limitations of the calorimetric method in a region such as ρ Ophiuchi, as discussed above. The same reason may explain the systematically lower values given by WLY to WL 2 and WL 10. The notes in the Appendix provide additional information on some sources.

TABLE 4

LOW-MASS STARS WITH THREE OR MORE MEASURED MAGNITUDES

Object	A_V	$L(L_\odot)$	$M(M_\odot)$	n
2303.6−1805......	23	0.04	0.08	−3.0
2314.4−1237......	18	0.9	0.8	−3.0
2315.8−1700......	44	0.6	0.41	−1.9
2317.3−1925......	10	0.07	0.13	−3.0
2317.5−1729......	16	0.05	0.09	−0.8
2320.0−1915......	3	0.06	0.11	−2.0
2320.8−1708......	17	0.1	0.18	−3.0
2320.8−1721......	5	0.003	0.02	−0.5
2321.2−1719......	13	0.004	0.02	−0.8
2321.6−1918......	22	0.02	0.04	−1.4
2322.8−1233......	31	0.04	0.08	−3.0
2324.1−1619......	22	0.09	0.15	−2.8
2326.5−1958......	7	0.04	0.09	−2.7
2330.1−1847......	14	0.15	0.22	−3.0
2331.1−1952......	16	0.04	0.09	−3.0
2346.8−2157......	33	1.0	0.61	−1.9
2355.7−2858......	35	0.4	0.47	−3.0
2357.3−2914......	23	0.3	0.39	−3.0
2404.5−2152......	15	0.02	0.06	−1.9
2407.3−2735......	13	0.8	0.51	−1.9
2408.5−2641......	23	0.3	0.36	−3.0
2408.6−2229......	11	0.01	0.04	−3.0*
2409.5−2807......	25	0.3	0.36	−2.0
2409.8−2611......	18	0.01	0.04	−1.6
2412.9−2447......	13	0.004	0.02	−2.5
2417.6−3500......	2	1.0	0.89	−3.0*
2417.7−2159......	35	1.0	0.59	−1.9*

* See Appendix.

Two very faint objects in Table 4, 2320.8−1721 and 2321.2−1719, are best fitted by a very low luminosity object with an amount of infrared excess typical of T Tauri stars. The best-fitting luminosities for these objects and for 2412.9−2447 fall below the grid of models of D'Antona & Mazzitelli (1985). For the sake of homogeneity, we have preferred not to use the lower mass models published by Nelson, Rappaport, & Joss (1986) for these fittings; instead, we have extrapolated the theoretical curves of D'Antona & Mazzitelli to include these objects. Moreover, the required temperatures are in a range where the atmospheric spectral features are poorly known. This makes rather uncertain the physical parameters listed for these objects. Rieke & Rieke (1990) included them in their list of candidate substellar objects in ρ Ophiuchi and assigned them a mass of $M \simeq 0.06\ M_\odot$. However, the apparent infrared excess may indicate a younger age. Furthermore, their colors seem to be redder than assumed by Rieke & Rieke and may have caused them to overestimate the extinction toward these sources. Both of these adjustments point toward masses lower than estimated by Rieke & Rieke.

Four other objects in Table 4 are also included in the list of low-luminosity objects of Rieke & Rieke (1990). They are 2321.6−1918, 2322.8−1233, 2408.6−2229, and 2412.9−2447. Our results indicate masses below 0.1 $M_\odot$ for all of them. Four more objects in Table 4 also seem to be below this limit: 2317.5−1729, 2326.5−1958, 2331.1−1952, and 2404.5−2152.

We have examined whether the low luminosities for these sources could result from use of an inappropriate extinction law to deredden them. Extinction with flatter wavelength dependence than in the general interstellar medium might result from the presence of large grains in the Ophiuchus dark cloud (e.g., Harris et al. 1978). Use of such a law tends to make our sources both more luminous at H, K, and L and redder in $J-H$ than assigned by us. Since $J-H$ should approximately represent the temperature of the underlying star (independent of infrared excess emission), the resulting trend—increased luminosity with decreased temperature—is contradictory to the expected behavior for realistic stars. Specifically, attempts to use a $1/\lambda$ extinction curve (as opposed to the normal curve's approximate $1/\lambda^2$ behavior) produce unacceptable dereddened spectral energy distributions for four of our very low luminosity objects—2321.2−1719, 2321.6−1918, 2408.6−2229, and 2412.9−2447.

For some objects in the region, measurements are available at only two wavelengths. In these cases, an upper limit to the luminosities can be obtained by assuming them to belong to class III. In Table 5, we list the objects for which these upper limits are within the low-mass region; the deduced extinctions and masses are also upper limits to the true values. Because of their faintness, most of the objects in Table 5 have not been identified in previous surveys. Many of the objects have upper limits to the mass placing them in the substellar range ($M < 0.085\ M_\odot$); this status nonetheless needs to be confirmed with more complete measurements. The faintest source in Table 5, 2321.1−1715, was considered by Rieke & Rieke (1990) as the most likely substellar object in their sample.

Given the various observational and modeling uncertainties, it is possible that some of the sources that appear to lie just below the stellar mass range are really stars. However, there are six sources with three or more colors and with assigned masses $\leq 0.04\ M_\odot$ and one with two colors and an assigned mass of $0.02\ M_\odot$. We have high confidence that most or all of these seven objects are substellar, since revisions by many times the estimated errors and uncertainties would be required to move them up to the stellar mass range, and we can identify no way that our methods would systematically underestimate the masses of all seven. These seven objects have derived luminosities a factor of 4 or more below that expected for the bottom of the main sequence (a factor of more than 5 below the main sequence if we had used the new models of Burrows et al. 1993). All seven of these objects were studied by Rieke & Rieke (1990), and six of them were suggested to be substellar by them on the basis of their photometric colors and brightnesses. We have estimated the mass of the seventh brown dwarf candidate from that paper to be $0.05\ M_\odot$.

The much more detailed analysis introduced in this paper derives somewhat lower masses than were previously assigned to these objects and points to additional substellar candidates. We showed in § 4.2.4 that the new analysis is robust to the observational errors. Similarly, it is robust to the presence of circumstellar dust, unless the excess radiation is at a temperature roughly 5 times lower than that of the primary object and the luminosities of the two source components are comparable. Many of these souces are too faint to search for such excesses, but the $K-L'$ photometry reported by Rieke & Rieke (1990) shows that excesses of 500 K or higher temperature with sufficient luminosity to produce a substantial underestimate of the primary source luminosity cannot be present for two objects, 2321.6−1918 and 2408.6−2229. The $K-N$ photometry in the same reference would also contradict the presence of sufficiently luminous excesses cooler than 500 K for two objects, 2320.8−1721 and 2408.6−2229. In § 4.2.4, we also report experiments that showed that the derived masses were robust against any plausible errors in the age estimate for the objects, largely because objects of age 2–5 × 10^6 yr and masses 0.02–0.05 $M_\odot$ are in a phase of deuterium burning that results in their luminosities being only a weak function of age. In § 4.1.3 we considered the reliability of the theoretical models of the substellar objects. A variety of potential sources of uncertainty were evaluated and found not to influence the models by factors nearly sufficient to result in assigning stellar masses (i.e., $M > 0.08\ M_\odot$) to these seven objects. In § 5.1 we demonstrated in detail that these objects are unlikely to be either foreground or background stars. We note that our analysis treats identical binaries as single stars with luminosity roughly twice that of each component, while the faint members of unequal binaries will be missed altogether; hence, we may be underestimating the number of low-luminosity objects in binary systems. Finally, in § 5.2 we show that the low-luminosity estimates for these sources are unlikely to result from errors due to an abnormal extinction law in the cloud.

TABLE 5

LOW-MASS STARS WITH ONLY TWO MEASURED MAGNITUDES

Object	A_V	$L(L_\odot)$	$M(M_\odot)$
2310.6−2001......	22	0.01	0.05
2311.0−1554......	35	0.15	0.21
2317.5−1630......	31	0.04	0.08
2318.4−1707......	29	0.01	0.04
2318.9−1740......	31	0.02	0.05
2320.0−1134......	37	0.07	0.12
2321.1−1715......	13	0.002	0.02
2322.3−1143......	10	0.009	0.04
2356.6−3058......	45	0.2	0.30
2403.7−2948......	45	0.2	0.27
2414.0−3159......	19	0.9	0.84
2416.9−2724......	28	0.02	0.06
2420.6−2254......	29	0.2	0.26
2431.5−3354......	39	0.09	0.15

5.3. *High-Mass Objects*

Several objects with bright infrared fluxes have been fitted as high mass objects, in or near the main sequence, and are shown in Table 6. All these objects have been reported in previous surveys, and many of them have been studied by other authors using different techniques, so that independent information is available on them which can be compared to our results, as indicated in the notes in the Appendix.

TABLE 6

HIGH-MASS STARS

Object	A_V	$L(L_\odot)$	n
2319.8−1617......	33	94	−2.1*
2332.6−1640......	14	1022	−3.0*
2400.8−3048......	31	57	−1.9*
2402.6−2146......	36	55	−3.0*
2413.8−3159......	23	51	−3.0*
2417.0−2221......	28	65	−3.0*
2419.6−3502......	40	124	−2.0*
2431.3−3435......	24	551	−3.0*

* See Appendix.

TABLE 7

INTERMEDIATE-MASS STARS

Object	A_V	n
2307.5−1206......	40	−3.0
2309.0−1411......	21	−1.9*
2315.3−1540......	11	−1.9*
2321.9−1415......	5	−1.2*
2322.6−1802......	10	−1.0*
2323.8−1801......	28	−3.0
2414.1−2408......	31	−2.2

* See Appendix.

5.4. *Intermediate-Mass Objects*

The six objects displayed in Table 7 are best fitted by a moderately hot star ($T < 10^4$ K) with an absolute Rayleigh-Jeans magnitude $M_{RJ} \sim 1.7$, as expected for intermediate-mass stars (1–3 $M_\odot$) in the process of developing a radiative core on their way to the main sequence. As explained before, we cannot determine luminosities for these stars because of their similar appearance at infrared wavelengths. Three of them show an appreciable amount of infrared excess, presumably corresponding to the less evolved members of this group. A short discussion of some of the objects is given in the Appendix.

Three other stars, listed in Table 8, have been observed at only two wavelengths and, as with the low-mass stars, only upper limits can be estimated for them. These upper limits place these objects in the intermediate-mass range, but some of them may actually have lower masses. On the other hand, the high extinction required to fit the observed magnitudes of 2316.0−1626 if considered as an intermediate mass star and the upper limit on the L' magnitude are compatible with its being a class I object. Two of the sources in Table 8 have been previously studied and are discussed in the Appendix.

5.5. *Class I Objects*

Since the nature of the class I objects prevents a detailed fitting of their photometry to a model, estimates of physical parameters in these cases are necessarily rough. We present in Table 9 the estimated luminosities and foreground extinction of 17 sources that we consider to be possible class I objects. To derive these quantities, a spectral index $n = 0.5$ has been assumed as a representative value for class I objects over the near-infrared range. For the more luminous sources, we consider that the calorimetric method provides a more reliable estimate of the luminosity; thus, we have listed in Table 9 the values given by WLY for these stars. Notes on some sources are in the Appendix.

In addition to some well-known possible protostellar objects reported in previous surveys, we have found a number of faint, very red sources which also show features of class I. Not all our classifications have the same reliability, however, because of the difficulties in obtaining unambiguous fits; particularly, the faintest two sources we have classified as class I, 2304.5−1657 and 2424.5−3759, are rather blue objects when compared to the rest of our candidates, and our classifications as class I objects arise in part as a consequence of our inability to fit them as low-mass emerged objects and the rough fulfillment of the condition of a steep rise in the near-infrared spectral energy distribution.

TABLE 8

POSSIBLE INTERMEDIATE-MASS STARS WITH ONLY TWO MEASURED MAGNITUDES

Object	A_V	n
2315.5−1337......	4	−2.5*
2316.0−1626......	50	−2.1
2328.9−1610......	27	−1.9*

* See Appendix.

TABLE 9

CLASS I OBJECTS

Object	A_V	$L(L_\odot)$
2304.5−1657......	5	0.2
2320.7−1803......	16	0.6
2323.8−1640......	26	2.1
2339.1−2032......	25	4.4
2341.1−1946......	24	3.0*
2341.1−1951......	13	0.9
2350.3−2357......	22	1.2
2351.8−2553......	22	1.7
2357.4−2816......	...	38[a]*
2407.8−3033......	...	48[a]*
2408.3−2315......	22	1.9
2416.1−2211......	22	8.9*
2416.6−3234......	22	2.7
2422.6−2248......	10	1.2
2422.8−3423......	54	9.3
2423.0−2256......	9	0.8
2424.5−3759......	1	0.1
2425.1−3410......	...	13[a]*

[a] Calorimetric luminosity taken from WLY.

* See Appendix.

5.6. *Completeness of the Survey*

Assuming a depth of $A_K = 6$ mag for the cloud, we can conclude that all the high- and intermediate-luminosity stars in the surveyed region have been detected down to $M_K \simeq 3.4$. For fainter stars, corresponding to masses $<0.4\ M_\odot$, the surveyed volume of the cloud becomes a function of the absolute magnitude of the star, since faint stars at the far edge of the cloud would be dropped below the detection limit of our survey by obscuration. Unfortunately, the precise amount of the necessary completeness correction depends on the detailed distribution of obscuring matter inside the cloud, for which our information is very limited. An estimate is however possible, by making the simple hypothesis that the depth of a star from the near surface of the cloud is proportional to the amount of extinction. In a survey limited by the magnitude $m_{K_{\rm lim}}$, a star with apparent magnitude m_K would then be visible over a volume

$$V \propto \min\,(A_{K_{\rm max}},\ m_{K_{\rm lim}} - m_K + A_K)\,, \qquad (13)$$

where $A_{K_{\rm max}}$ is the total K extinction of the cloud. The number density of a group of i stars of different apparent magnitudes and extinctions is then

$$n \propto \sum_i \frac{1}{V_i}\,. \qquad (14)$$

We have calculated in this way all the space densities appearing in the following discussion. The actual proportionality factor in formula (14) is unknown; nevertheless, we do not need it since we are mainly interested in density ratios.

The uncertainty in the star number density n is difficult to estimate, given the different nature of the contributing factors (adopted stellar models, photometric precision, hypotheses on the distribution of dust in the cloud, etc.). The error bars in our figures are given by

$$\sigma^2(n) \propto \sum_i \frac{1}{V_i^2} \tag{15}$$

which, for a set of N identical sources, would simply give the number density as $(N \pm N^{1/2})$. Below a mass of 0.4 $M_\odot$, the completeness corrections introduce additional uncertainties which are difficult to quantify. However, these corrections are sufficiently small for $M > 0.1\ M_\odot$ that the statistical errors are likely to dominate.

5.7. *Evolutionary Time Scales of the Different Classes of Objects*

Assuming a constant star formation rate in the ρ Ophiuchi cloud over the last 3.5×10^6 yr, the number densities of each spectral index class should be a measure of the duration of each phase, if we accept the spectral index as an indication of the evolutionary status of an object. A first estimate of the duration of phase p is given by the simple relation

$$t_p = \frac{n_p}{n_{\rm tot}}\, t_c\ , \tag{16}$$

where n_p is the number density of objects in phase p, $n_{\rm tot}$ is the total number density of objects, regardless of their evolutionary phase, and t_c is the age of the star-forming region. In writing equation (16), we neglect the fact that objects with different masses can be expected to have different evolutionary timescales. Given the low number of available objects for our statistics and the simplifying hypotheses we have been forced to make, we consider it unnecessary to introduce such refinements.

Moreover, in relating the number density of objects with the duration of each phase by means of equation (16) we do not take into account that an enhanced space density as deduced from our sample can arise from the fact that some of the objects may be brighter while in their early phases, then fade below the limit of detectability of our survey when they are more evolved. We do not expect this to have a strong effect on our class II and class III objects, because their brightnesses at near-infrared wavelengths are not likely to have changed very substantially over the lifetime of the ρ Ophiuchi region. However, our results show that the same does not seem to hold for class I objects. Direct application of equation (16) to them gives $t_I = 1.1 \times 10^6$ yr, that is, an age in excess of 10^6 yr for the duration of the embedded phase, or even more if we include some of the stars that were considered as possible background. Both observational (Cohen & Kuhi 1979) and theoretical (Stahler 1983) arguments place the birthline of T Tauri stars at a much younger age than this, about 1.5×10^5 yr. This discrepancy suggests the existence of a selection effect in our sample (or a bias in our analysis) toward class I objects.

It is easy to show that, if we accept the birthline of T Tauri stars as an upper limit to the age of our class I objects, the less luminous objects we have found should have masses as low as the faintest class II and class III objects. The luminosity emitted by an accreting protostar is mostly due to the release of potential energy by the infalling material, with only a small fraction coming from the embedded object (Stahler, Shu, & Taam 1980). Thus, we can write

$$L = \frac{GM\dot{M}}{R} \tag{17}$$

for the luminosity of a class I object with a mass M and a radius R accreting material at a rate $\dot{M}$. If the accretion from the surrounding medium takes place at a constant rate, then $\dot{M} = M/t$, and

$$M = \sqrt{\frac{LRt}{G}}\ . \tag{18}$$

A typical value for the radius of a low mass embedded protostar is $R = 3\ R_\odot$ (Stahler et al. 1980), and it does not have a strong dependence on the mass, so that, for $t = 1.5 \times 10^5$ yr, equation (18) becomes

$$M = 0.12\sqrt{L} \tag{19}$$

expressing M in $M_\odot$ and L in $L_\odot$. Taking into account that, for some sources, L seems to be below 1 $L_\odot$ and that equation (19) gives an upper limit to M, it seems likely that some of our class I objects may have very low masses, and they might have escaped detection had they evolved past the protostellar phase. On the other hand, equation (19) can be interpreted as a mean mass-luminosity relation when an average value of the age of the objects is used.

If we assume a duration of $t_I = 1.5 \times 10^5$ yr for the embedded phase, a constant formation rate, and a similar degree of completeness for our samples of class II and class III objects, we obtain for the duration of the T Tauri phase:

$$t_{II} = \frac{n_{II}}{n_{II} + n_{III}}\,(t_c - t_I)\ . \tag{20}$$

The result is $t_{II} = 1.15 \times 10^6$ yr, thus placing the transition from class II to class III at $t_I + t_{II} = 1.3 \times 10^6$ yr. The statistics on the abundance of different classes of objects are shown in this way to be consistent with the representative ages for the different kinds of objects that we have assumed at the beginning. The value of 1.3×10^6 yr is also in good agreement with the age derived by WLY for their oldest T Tauri star and with the position of the known T Tauri stars in the H-R diagram (Bertout 1989).

In the Taurus region, Strom, Edwards, & Skrutskie (1990) estimate that half of the stars younger than 3×10^6 yr are surrounded by optically thick disks; the reradiated spectrum from the disk dominates the stellar output for $\lambda > 4\ \mu$m. Walter et al. (1988) suggest that conventional search methods may overestimate the portion with substantial circumstellar material, so the estimate of Strom et al. may be an upper limit. Nonetheless, it is noteworthy that our derived spectral indices have a very similar distribution, with the objects divided equally between classes II and III.

The test discussed above based on the relative numbers of embedded objects and the comparison with the Taurus region both support the age estimates used in our analysis and would not be consistent with the source population being as old as 10^7 yr.

5.8. *Luminosity and Mass Functions*

5.8.1. *Power-Law Fits*

Given the uncertainties in the interpretation of infrared observations, care has to be taken to construct an unbiased luminosity function. Our procedure has been as follows:

1. We have excluded from consideration class I objects, since the luminosity of the central source cannot be reliably evaluated from the observed accretion luminosity and, moreover, the latter is estimated to a very limited degree of accuracy.

2. We have divided our stellar objects into six bins: two for the high-mass stars, separated at $L = 100\ L_\odot$ and considering the lower end to be $50\ L_\odot$; one for the intermediate-mass stars, for which the resolution of our method is poor as discussed above; and three for the low-mass objects, which constitute most of our sample and for which our method is expected to work relatively well.

3. We have included in the luminosity function those stars for which only two colors are available, to avoid a bias toward high-luminosity objects that have been measured at more wavelengths on the average. The luminosities of the low-mass stars in this category have been taken as their upper limits, obtained by assuming them to belong to class III. This procedure may overestimate the true luminosity of these objects; however, given the fact that $\frac{3}{4}$ of the low-mass stars with three or more measured magnitudes are indeed class III, we do not expect this to be an important distorting factor. The same holds for stars with only H and K magnitudes that we have classified as possible intermediate-mass stars; we have included them in the intermediate-mass bin. In any case, their small number minimizes the possible biases coming from this choice.

The space density of the stars in the different bins is represented in Figure 3. We have fitted a theoretical curve to these results by assuming that the space density–luminosity relationship can be written as a power law:

$$n(L)dL = AL^b\,dL\ , \tag{21}$$

where $n(L)$ is the number density of stars with luminosities between L and $L + aL$. We get a best fit by taking $b = -1.21$. It is difficult to ascertain whether the deviations from the power law in Figure 3 arise from the uncertainties in our results or reflect real deviations from the proposed shape in the ρ Ophiuchi region. Although our results do not show an indication of a decrease in the faint end of the luminosity function, the actual shape at low luminosities is necessarily uncertain. For high- and intermediate-mass stars, the contraction toward the main sequence may be considered to take place with a constant luminosity as a first-order approximation, the luminosity function therefore being fairly independent of the evolutionary status. Nevertheless, fully convective stars monotonically decrease their luminosities as they contract and, as a result, the luminosity function in these regions becomes noticeably time-dependent, the shape of the luminosity function depending both on the main-sequence luminosity function and on the ages of our stars.

It is then useful to investigate the behavior of the mass function instead of the luminosity function, as a time-independent characterization of the distribution of stellar parameters at the low-mass end. The assignment of masses to the stars is to some extent dependent on the isochrones used; however, this dependence is weak enough so as not to alter our results significantly.

Our procedure in fitting a power law to the initial mass function has been essentially the same as with the luminosity function. The bins for the high- and intermediate-mass stars are conserved; by using a standard mass-luminosity relationship for main-sequence stars (Allen 1973) in the high-mass range, the bin limits are now $3.8 < M < 7.5\ M_\odot$ and $3 < M < 3.8\ M_\odot$. The intermediate-mass bin is considered to consist of stars with $1 < M < 3\ M_\odot$. The low-mass bins are rearranged since, by the use of two different isochrones, there is not a one-to-one correspondence between luminosity and mass; we have thus used the bins $0.4 < M < 1\ M_\odot$, $0.1 < M < 0.4\ M_\odot$ and $0.02 < M < 0.1\ M_\odot$.

Our best fit to the power law

$$n(M)dM \propto M^c\,dM \tag{22}$$

is obtained with an exponent $c = -1.14$. The formal error in this exponent is 0.2. In Figure 4, we plot the distribution of masses per logarithmic mass interval and compare with the fit in formula (22). Some departures appear from the mean power law also in the mass function, mainly consisting of an excess at masses around $3\ M_\odot$. This result must be taken with caution, as shown by its large error bar, because the statistics at high mass are based on a low number of objects, and the possibility of misclassification of some of them is not excluded.

A comparison that illustrates that the power-law fit is not strongly affected by completeness corrections for the lowest mass bin can be made by normalizing the power law to the mass range 0.4–7.5 $M_\odot$, over which no corrections were made, and predicting the number of objects in the 0.02–0.1 $M_\odot$ bin. In this way, we predict 24 objects in the lowest mass bin, and we have detected 19. Therefore, the data show no reduction in slope near the bottom of the main sequence. With complete-

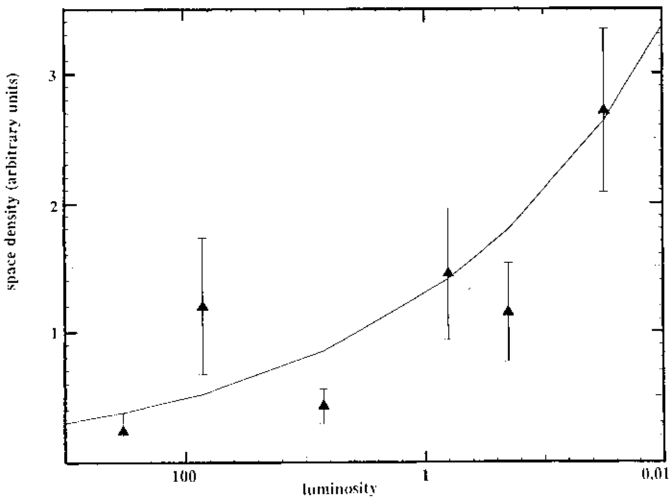

FIG. 3.—Luminosity function for class II and class III sources

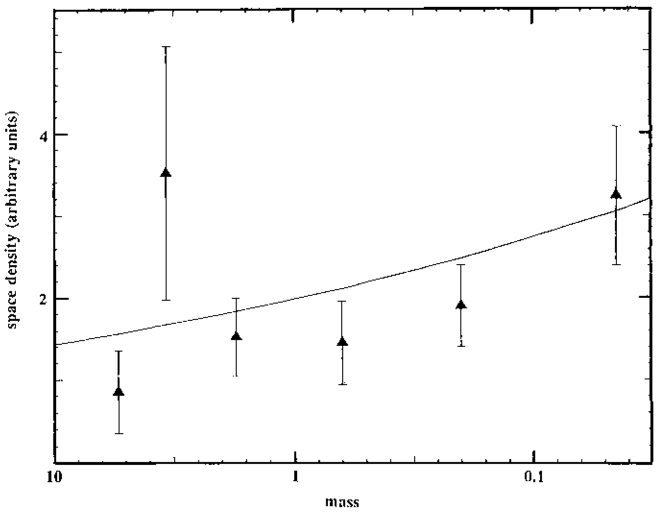

FIG. 4.—Mass function for class II and class III sources

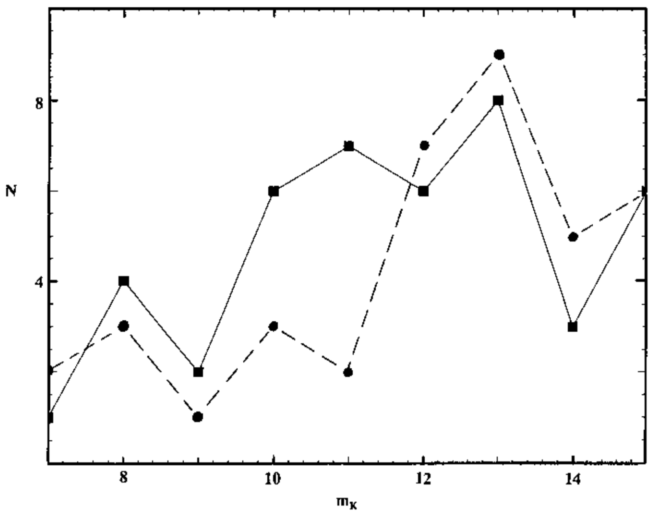

FIG. 5.—Comparison between the K magnitude distribution of the two major molecular concentrations in the ρ Ophiuchi core. A rough extinction correction has been applied to the observed K magnitudes by assuming $K = K_{obs} + 0.54 - 1.8(H-K)_{obs}$.

ness corrections, there is a hint of an increase in slope at the low-mass end of the sample, to ~ -1.3 (see Fig. 4). However, this latter result is quite uncertain because the increase is in the direction that would result from errors in the completeness correction caused by nonuniformities in extinction.

The slope of our derived mass function may be somewhat contaminated by undetected binaries, as discussed by Reid (1987), since our analysis treats binaries as a single star of roughly the total luminosity of the pair. Because of the shallow dependence of mass on luminosity and the breadth of the mass bins we have used, binaries of roughly equal mass would result in a bias only if the incidence of such systems were a function of the mass. However, as in all studies of this type, binaries of unequal mass will be counted only as a single star of the dominant type. Hence, our derived IMF may underrepresent the number of low mass stars.

The slopes we have derived from fitting the IMF are consistent with recent determinations of the local IMF and the IMF in clusters from 0.1 to 1 $M_\odot$ (e.g., Reid 1987; Tinney, Mould, & Reid 1992; Laughlin & Bodenheimer 1993). However, in this case the IMF extends significantly below the bottom of the main sequence, with no apparent deviation from this power law. The power-law fit is uncertain both from the standpoint of limited statistics and the number of assumptions in reaching it. However, the basic conclusion rests on the large number of substellar objects listed in Tables 4 and 5.

We find a relatively large number of moderate-mass stars compared with the classical power-law exponent of -2.35 derived by Salpeter (1955) and with the Miller & Scalo (1979) IMF for the range $0.4 < M < 10\ M_\odot$, a result that seems to be consistent with other more recent studies at least above 1 $M_\odot$. The small value of the low-mass–to–high-mass star number density ratio as compared with standard shapes of the initial mass function is also in agreement with the effects predicted by the theory of star formation of a sensitivity of the mass spectrum to the conditions of the star-forming cloud (Larson 1985, 1991). Evans & Lada (1991) have compared the star formation in the Orion, Taurus, and ρ Ophiuchi molecular clouds, and the differences between the luminosity functions in the Taurus-Auriga molecular complex and ρ Ophiuchi have been discussed by Elias (1978b) and Kenyon et al. (1990). Elias (1978b) proposed a supernova explosion as the triggering mechanism of star formation in ρ Ophiuchi, which would have proceeded in a more quiescent way in Taurus leading to the predominance of lower masses. Such catastrophic events may not be required, however, in view of the proximity of ρ Ophiuchi to the association Scorpius OB2. Evidence exists for sequential star formation in Scorpius OB2 toward the direction of ρ Ophiuchi (Blaauw 1991; de Geus, de Zeeuw, & Lub 1989). As shown by Elmegreen & Lada (1977), sequential star formation in molecular clouds tends to form massive stars as a result of the higher gas temperatures. Temperatures in ρ Ophiuchi have indeed been found to be in excess of 30 K (Loren, Sandqvist, & Wooten, 1983), thus placing it in the warm cloud population described by Solomon, Sanders, & Rivolo (1985).

The fact that the differences in the stellar populations of different clouds reflect variations in the star-forming processes rather than evolutionary effects is supported by the similarity between the stellar populations of two "quiescent" molecular clouds, Taurus and Chamaeleon, whose ages are younger and older than that of ρ Ophiuchi respectively (Gauvin & Strom 1992).

5.8.2. *Local Variations in the Luminosity Function*

Barsony et al. (1989) suggest that the luminosity function may vary within the ρ Ophiuchi molecular cloud. Our new data allow a second test of this hypothesis. Figure 5 compares the distribution of dereddened K magnitudes for the southeast cloud peak with that for the northwest one. In this comparison, we have rejected all sources with $H-K > 3.0$ or $H-K < 0.5$ (the latter condition applies to two sources which may be foreground). No corrections other than dereddening were applied. As shown in Figure 5, there is a suggestion that the distribution of m_K is deficient in low-luminosity objects in the southeast peak, as originally suggested by Rieke et al. (1989), whereas there are many such objects in the northwest peak. We should point out that the relative densities of class I, class II, and class III objects do not differ significantly between the two concentrations, thus indicating that the differences in the source counts are not a consequence of a difference in the evolutionary stages of the two peaks.

To see if this difference actually represents a significant difference in the luminosity functions in these areas, or is just a statistical anomaly, we have used the Kolmogorov-Smirnov test to compare the two distributions. It indicates a 93% probability that the intrinsic luminosity distributions are different. Thus, although not at a high level of statistical confidence, our data suggest that there may be real differences in the two luminosity functions. This result supports the argument of Barsony et al. (1989) that determination of unbiased luminosity distributions may require mapping of large areas (and possibly many clouds) to sample the results of a variety of star formation conditions.

6. ADDITIONAL REMARKS

One year after the original survey, source 2418.4−3008 could not be detected to a level at least 1.5 mag fainter than its listing in Table 1. This object was also not detected in the survey of Barsony et al. (1989), 1 year previous to our survey. We examined our data and discovered that the brightness of the source fluctuated by a factor of 2 during the 20 minutes in which we observed it. The detection in this survey appears to apply to a flare. We note that flaring activity in the X-ray is

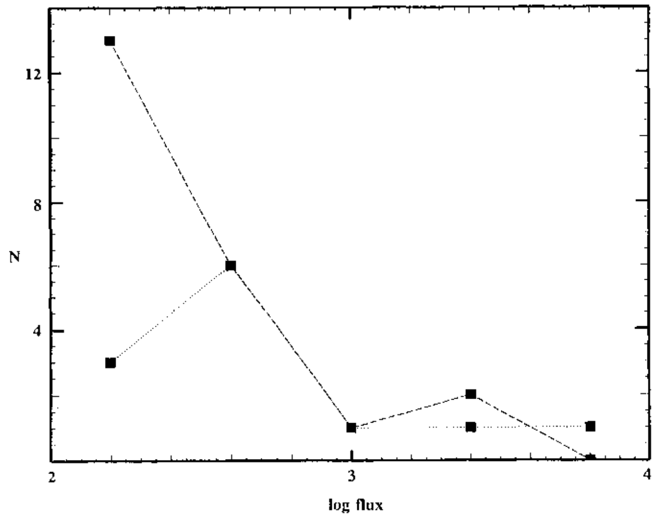

FIG. 6.—Distribution of fluxes (in mJy) at 6 cm for the souces detected (*dotted line*) and undetected (*dashed line*) in our survey. Data were taken from Leous et al. (1989).

common for embedded sources (Montmerle et al. 1983) and is seen in the radio in some instances (Stine et al. 1988). Three years after its initial detection, 2313.3−1421 was found to be about 1.3 mag fainter than its initial detection and below the detection threshold of the initial survey; it is therefore another candidate for large-amplitude variability.

It is likely that some very faint sources represent star formation occurring deep within or on the opposite side of the cloud. Evidence for this possibility can be obtained from a comparison of the radio and infrared source populations. Although 14 of the infrared sources are identified with radio sources in the deep VLA map of Leous et al. (1989), there are a total of 23 radio sources in the region mapped in the infrared. The radio luminosity functions of the detected and undetected source populations are different, as shown in Figure 6. These results suggest two possibilities. First, some of the faintest radio sources may not be associated with the molecular cloud; equally deep mapping of control fields in the same direction could test this hypothesis. Second, our images may only detect about half of the embedded sources. For example, there may be low-luminosity sources on the far side of the cloud that are too heavily obscured for detection at K.

7. CONCLUSIONS

We report a near-infrared survey of 200 arcmin^2 in the cores of the ρ Ophiuchi interstellar clouds. Our analysis of these data shows the following:

1. Ninety-one sources have been found, of which nearly all are physically associated with the region of star formation in these clouds.
2. Calorimetric methods of estimating luminosities of dust embedded sources are not applicable to the low-luminosity members of this population.
3. A new method based on fitting of isochrones from theoretical models appears capable of giving reliable luminosity estimates for objects with masses less than about one solar mass.
4. Application of this method allows us to determine a luminosity function and accompanying initial mass function for the cluster of young stars forming in these clouds.
5. The IMF extends to well below the bottom of the main sequence (0.08 $M_\odot$) with no obvious feature at the transition between stellar and substellar masses.
6. The power-law exponent of the IMF is roughly −1.14, consistent with extrapolation of many estimates of the local IMF to substellar masses.
7. At least seven objects appear to be substellar, even allowing for the largest plausible errors in the observations, the analysis, and the theoretical evolutionary models for these sources.
8. One source was detected in a bright flare and additional sources may be large-amplitude variables.

This search seems to detect very young, brown dwarfs at about the frequency expected from an extrapolation of the local IMF toward substellar masses. It therefore seems likely that brown dwarfs form in significant numbers and that the process of cloud fragmentation is not biased against substellar masses. The difficulties in detecting older brown dwarfs are probably a result of rapid cooling and possibly of the formation of atmospheric absorptions that may depress their near infrared output spectra.

We are grateful to W. T. Morgan for the reduction of the survey observations. We thank the Vatican Observatory and particularly C. Corbally for support and hospitality. We appreciate discussions with T. P. Greene, W. B. Hubbard, J. Lunine, D. Saumon, J. Stauffer, and E. T. Young. Assistance at the telescope was provided by H. Campins, T. P. Greene, B. Wilking, and E. T. Young, and by J. McAfee, D. Means, and G. Rosenbaum. A. B. acknowledges support from NASA (NAGW-2145) and NSF (AST89-14346). The work of G. H. R. and M.J.R. was also supported by NASA (NAGW-2606) and NSF (AST-9116442). The contributions of F. C. were supported by the Spanish Plan Nacional de Formación de Personal Investigador.

APPENDIX

NOTES ON INDIVIDUAL SOURCES

2309.0−1411 = GSS 26 is considered to be class II by WLY, who give a luminosity $L = 0.7\ L_\odot$ from calorimetric estimates. The object may be somewhat more luminous given the limitations of these estimates.

2315.3−1540 = GSS 29 = E118 has a class II spectral index, according to WLY, consistent with the infrared excess that we find. The object appears bright as a consequence of the low extinction toward it, and its luminosity does not seem to be much higher than that given by WLY, $L = 0.8\ L_\odot$.

2315.5−1337 = ROX 10A = E119 is a bright source with a small amount of extinction. Photometry in optical wavelengths was obtained by Bouvier & Appenzeller (1992), who also detected strong Hα emission and classified it as a K5 star; it thus seems to be a class II source on the border between low- and intermediate-mass objects.